# Phonon frequencies for Si-Ge strained-layer superlattices calculated in a three-dimensional model

R. A. Ghanbari,* J. D. White, and G. Fasol
*Cavendish Laboratory, University of Cambridge, Madingley Road, Cambridge CB3 0HE, England*

C. J. Gibbings and C. G. Tuppen
*British Telecom Research Laboratories, Martlesham Heath, Ipswich, IP5 7RE, England*
(Received 2 March 1989; revised manuscript received 19 April 1990)

We present the results of full three-dimensional calculations of phonon frequencies in silicon-germanium strained-layer superlattices (SLS's) and compare with experimental data. We use a modified version of the six-parameter valence-force-potential model, incorporating the strained nature of the layers. We confirm that the dispersion relations for Si/Ge SLS's fall into bands closely associated with the bulk dispersion relations of silicon and germanium, as expected. Also, we find that our model precisely reproduces the predicted strain-induced frequency shifts to within one-tenth of 1% for epitaxial layers grown in the [001] direction, if longitudinal and transverse polarized phonons are considered separately. We also present analytical expressions for these frequency shifts. We find that the degree of penetration of confined LO phonons into adjacent layers is qualitatively different for growth in the [001] and [110] directions. Confined phonons in [110] superlattices have nearly zero penetration depth into adjacent layers, while the penetration depth for phonons in [001] superlattices is quite significant. This large penetration depth for [001] superlattices allows for coupling of transverse interface modes across thin layers, giving rise to a bifurcation of these otherwise degenerate modes. We also show that only transversely polarized interface modes are confined to the interface region, while longitudinally polarized modes with similar energies actually extend across the silicon layers and thus depend strongly on the width of the silicon layers. We compare our calculated results with measured Raman spectra of two typical samples and find that our model gives the correct position of the Raman peaks to within 1 $cm^{-1}$, after correcting for temperature.

## I. INTRODUCTION

Currently there is great interest in the study and characterization of silicon-germanium strained-layer superlattices (SLS's), fueled by the hope of introducing heterostructure capabilities to the silicon system.[1] For $GaAs/Al_xGa_{1-x}As$ superlattices, luminescence has been an important characterization technique. Si/Ge superlattices and quantum wells are known to show luminescence only under special conditions,[2] making Raman spectroscopy a valuable characterization technique for the Si/Ge system. Raman measurements of folded acoustic phonons yield the period length, and the position of the $n=1$ confined phonons yields the strain.[3-5] The Raman strength of the Si/Ge interface phonon modes has recently been related to the amount of interface disorder.[6,7]

For detailed interpretation of Raman spectra, it is necessary to calculate the vibrational spectra. Fasolino *et al.*[8] have made phonon calculations for Si/Ge SLS's using a linear-chain calculation in which the lattice planes are replaced by equivalent atoms on a one-dimensional linear chain. This model was used to show confined phonons and interface phonons and is in qualitative agreement with Raman experiments. However, in order to quantitatively model the phonon dispersion relations and to calculate other three-dimensional properties (such as the phonon dispersions in arbitrary directions, Raman spectra, and the phonon density of states), a fully-three-dimensional (3D) model incorporating strain effects is required. Phonon calculations in fully 3D models have been introduced only recently to model the Si/Ge superlattice system.[9,10] Alonso *et al.*[10] have implemented a two-force-constant Keating model to qualitatively model Si/Ge superlattices and investigate the symmetries of the superlattice phonon modes. Recent calculations have attempted to investigate the effect of interface roughness on the Raman spectrum of $(Si)_4/(Ge)_4$ superlattice[11,12] and to calculate Raman intensities.[11]

In the present work we present calculations of phonon frequencies for the Si/Ge system using a modified version of the six-parameter valence-force-potential model[13] (VFPM) to incorporate strain effects.[9] The VFPM has been used successfully to *quantitatively* model the bulk phonon dispersion relations of many materials such as silicon, germanium, and Hittorf's phosphorus.[14,15] In our implementation we take account of both strain-induced lattice distortions and the changes in interatomic interactions due to strain, which cannot be readily done with other methods.

With our model we find that transverse polarized interface modes and the longitudinally polarized mode with approximately the same energy behave quite differently,

 

with the transverse modes being confined to the interface region. Also, we studied the behavior of confined phonons. There has been some question recently whether the energies of confined phonons in GaAs/AlAs quantum wells, when plotted against the "confinement wave vectors," ought to follow the bulk-phonon dispersion.[16–18] We use our model to predict a deviation from the bulk-phonon dispersion for a Si/Ge superlattice grown in the [001] direction, with negligible deviation for Si/Ge superlattices grown in the [110] direction. This is consistent with recent measurements on [110] Si/Ge SLS's.[19] We also present measured Raman spectra for $(Si)_4/(Ge)_4$ and $(Si)_8/(Ge)_4$ superlattices, and show that the position of the Raman peaks corresponds to those predicted by our model to within 1 $cm^{-1}$, after adjusting for temperature.

## II. THEORY

The presence of strain in Si/Ge SLS's disrupts the cubic symmetry of the different layers by distorting the layers differently in the in-plane and growth directions. This distortion causes a shift in the observed phonon frequencies from what would be expected in an unstrained system.[20] It can be shown[21] that for the triply-degenerate optical modes at $\mathbf{k}\approx\mathbf{0}$, the frequency shifts can be calculated by solving the secular equation

$$\begin{vmatrix} p\epsilon_{xx}+q(\epsilon_{yy}+\epsilon_{zz})-\lambda & 2r\epsilon_{xy} & 2r\epsilon_{xz} \\ 2r\epsilon_{xy} & p\epsilon_{yy}+q(\epsilon_{xx}+\epsilon_{zz})-\lambda & 2r\epsilon_{yz} \\ 2r\epsilon_{xz} & 2r\epsilon_{yz} & p\epsilon_{zz}+q(\epsilon_{xx}+\epsilon_{yy})-\lambda \end{vmatrix} = 0 , \tag{1}$$

where $\lambda=\Omega^2-\omega_0^2$ ($\Omega\approx\omega_0+\lambda/2\omega_0$ being the phonon frequency under strain and $\omega_0$ the unstrained frequency), $\epsilon_{ij}$ are the strain components with notation referred to the crystallographic axes $x=[100]$, $y=[010]$, and $z=[001]$, and $p$, $q$, and $r$ are known phenomenological parameters fitted to experiment.

If the frequency shifts are sufficiently small, it can be readily shown that the frequency shifts predicted by Eq. (1) for films grown in the [001] direction are approximated by the relations

$$\delta\omega_T=\frac{p+q(K_{[001]}+1)}{2\omega_0}\epsilon_{lat} \tag{2a}$$

and

$$\delta\omega_L=\frac{K_{[001]}p+2q}{2\omega_0}\epsilon_{lat} , \tag{2b}$$

where $\delta\omega_T$ is the frequency of the two degenerate transverse-optical modes at $\mathbf{k}\approx\mathbf{0}$, $\delta\omega_L$ the frequency shift of the longitudinal-optical mode at $\mathbf{k}\approx\mathbf{0}$, $\epsilon_{lat}$ is the lateral strain in the layer given by the relation

$$\epsilon_{lat}=\frac{a_{sub}-a_0}{a_0} , \tag{3}$$

where $a_0$ is the unstrained bulk lattice constant of the strained layer and $a_{sub}$ is the lateral lattice constant of the buffer layer, and where $K_{[001]}$ is the proportionality constant which relates strain in the [001] growth direction to strain perpendicular to the growth direction ($\epsilon_{lat}$). Using stress-strain relationships and imposing symmetry considerations, it can readily be shown that

$$K_{[001]}=-2\frac{C_{12}}{C_{11}} , \tag{4}$$

where $C_{ij}$ are the bulk elastic stiffness constants in standard notation.

Similarly, for SLS's grown in the [110] direction, the calculated frequency shifts from Eq. (1) can be shown to be

$$\delta\omega_1=\frac{p(K_{[110]}+1)+q(K_{[110]}+3)+2r(K_{[110]}-1)}{4\omega_0}\epsilon_{lat} , \tag{5a}$$

$$\delta\omega_2=\frac{p(K_{[110]}+1)+q(K_{[110]}+3)-2r(K_{[110]}-1)}{4\omega_0}\epsilon_{lat} , \tag{5b}$$

and

$$\delta\omega_3=\frac{p+q(K_{[110]}+1)}{2\omega_0}\epsilon_{lat} . \tag{5c}$$

where

$$K_{[110]}=-\left[\frac{C_{11}+3C_{12}-C_{44}}{C_{11}+C_{12}+C_{44}}\right] . \tag{6}$$

Note that a given lateral strain causes the triple degeneracy at $\mathbf{k}\approx\mathbf{0}$ to split into three different frequencies for layers grown in the [110] direction, as opposed to two different frequencies in the [001] case.

## III. COMPUTATIONAL PROCEDURE

For this work, we used a version of the six-parameter valence-force-potential model[13] modified to incorporate strain effects and the superlattice structure. This model calculates the vibrational modes of the lattice by using the valence-force-energy function of the crystal lattice and assumes the atoms to be point masses with the interatomic forces approximated by Hooke's law. The primary criticism of this model involves its emphasis on short-range interactions, while neglecting long-range electro-

static effects which are essential when modeling such materials as BeO and GaAs. However, it is generally agreed that long-range electrostatic forces, such as Coulomb forces, have minimal impact on the vibrational properties of silicon and germanium lattices.[22]

The basic cellular binding block used in this work is shown in Fig. 1. This unit cell is one of the many possible primitive cells of a four-layer, diamond structure grown in the [001] direction, and it is also the primitive cell for a two-layer superlattice grown in the [110] direction. Strain effects on the Cartesian coordinates were incorporated by setting the lateral lattice constants of all layers to that of the buffer layer and adjusting the lattice constant in the growth direction such that

$$a_G = K(a_{\text{sub}} - a_0) + a_0 \ , \tag{7}$$

where $a_G$ is the lattice constant in the growth direction and $K$ is the appropriate strain proportionality constant from Eq. (4) or (6), depending on the growth direction. The valence coordinates remain unchanged in strained systems.

The values for the six different valence-force constants for bulk silicon and germanium used in our model are taken from Tubino *et al.*[15] who fitted the calculated phonon dispersions to data from neutron-scattering experiments done at room temperature. Strain affects the values of these bulk force constants by changing the interatomic distances and angles from their bulk equilibrium values. Cerdeira *et al.*[23] have presented arguments indicating that the angular dependence of these force constants is minimal. However, the force constants scale with changes in interatomic distances to a very high power. For this work, we assumed (after Cerdeira *et al.*[23]), that all force constants scale to the same power with changes in interatomic distances, such that

$$F = F_0 \left[ \frac{r}{r_0} \right]^n \ , \tag{8}$$

where $F_0$ is the force constant of the unstrained bulk, $r_0$ is the unstrained bulk interatomic distance, $r$ is the interatomic distance when strained, and $n$ is a fit parameter. Any strain-induced angular dependence of the force constants was neglected.

The force constants for interactions across the interface between the silicon and germanium layers were taken arbitrarily to be the average of the strain-adjusted force constants of the bulk materials. However, it was found that the averaging scheme used at the interface was generally unimportant because most phenomena involving the interface are primarily due to differences in the atomic masses of the materials rather than differences in atomic-interaction terms.[24]

The phonon density of states (DOS) of the structures were calculated by diagonalizing the dynamical matrix at random points throughout the primitive zone in **k** space. A sufficient number of points was used to ensure convergence. The eigenfrequencies were tallied in a histogram to give the phonon DOS as a function of wave number.

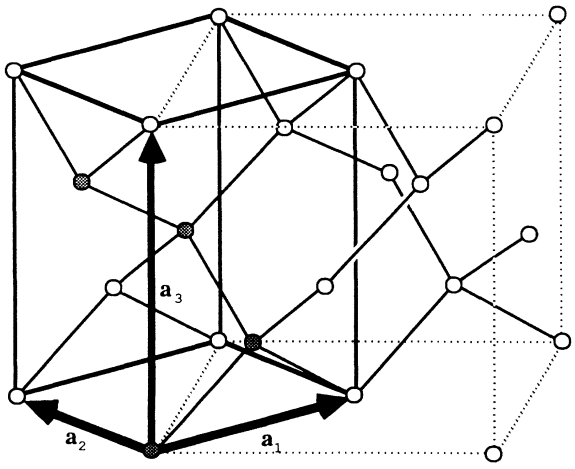


FIG. 1. Unit cell used to generate superlattices in the [001] ($\mathbf{a}_3$) and [110] directions ($\mathbf{a}_1$). The shaded atoms are the four atoms in the unit cell. Note that there are two atoms per plane in the [110] direction and only one atom per plane in the [001] direction.

## IV. RESULTS AND DISCUSSION

### A. Inclusion of strain

To incorporate strain into our calculations, it was necessary to first obtain the scaling parameter, $n$, used to modify the force constant in Eq. (8). For [001]-oriented layers we found that two different values of $n$ ($n_T$ and $n_L$) were necessary to give the frequency shifts predicted by Eqs. (2a) and (2b), respectively.[9] However, we found that if we calculated longitudinal and transverse modes separately using the appropriate scaling parameter, our model gave the linear frequency shifts of zone-center phonons predicted by Eqs. (2) to within one-tenth of 1% for all substrate lattice constants between 5.43 Å (pure Si) and 5.66 Å (pure Ge) for both silicon and germanium epitaxial layers. Table I lists the parameters used in this work.

We were unable to successfully include strain in our model for [110]-oriented layers. For this growth direction, biaxial strain causes there to be different bond lengths, depending on the crystallographic orientation of the bond. Because some of the valence-force constants

TABLE I. Parameters for Si and Ge used in this work.

| Parameter | Si | Ge | Units | Ref. |
|---|---|---|---|---|
| $C_{11}$ | 16.57 | 12.89 | | |
| $C_{12}$ | 6.39 | 4.83 | $10^{11}$ dyn/cm$^2$ | 29 |
| $C_{44}$ | 7.96 | 6.71 | | |
| $p$ | −1.43 | −0.47 | | 30 (Si) |
| $q$ | −1.89 | −0.6167 | $10^{28}$ s$^{-2}$ | 22 (Ge) |
| $r$ | −0.59 | −0.2775 | | |
| $n_T$ | −6.015 | −6.43 | | |
| $n_L$ | −3.095 | −2.94 | | 9 |

couple several bonds, we could not devise a method to utilize Eq. (8) that had any physical basis. Thus, we neglect strain in our modeling of [110] superlattices.

### B. Calculated dispersions

Figure 2 shows the calculated phonon dispersions of a $(Si)_4/(Ge)_4$ superlattice grown on a [001] silicon substrate. The phonon DOS is shown on the right-hand side of the figure. The dispersions for this structure can be broken up into three distinct frequency regions, as shown in the figure. It is important to note that the dispersion relations in the [ζ00] direction (in-plane direction) were calculated using the scaling parameter for longitudinal modes ($n_L$), as these are the modes that are usually observed experimentally. For modes propagating in this direction, the transverse and longitudinal modes are no longer decoupled, and, therefore, cannot be modeled separately. This introduces a slight error in these dispersions, but does not affect the qualitative behavior of the in-plane dispersion relations or the phonon DOS.

In the longitudinal polarization there are two modes within region I. They show no dispersion throughout the zone, indicating confinement. From the eigenvectors it is found that they are confined to the silicon layer, having very little amplitude in the surrounding germanium layers. Their properties are derived from the bulk silicon longitudinal-optical (LO) phonons. In the transverse polarization, there are three modes in region I, all derived from the bulk silicon transverse-optical (TO) phonons. Again, they have flat dispersions, indicating confinement within the silicon layer. In the [ζ00] direction both the LO and TO modes show some dispersion, indicating that confinement effects of the superlattice do not apply to phonons in this direction. The DOS shows a distinct peak in this region due to the confined phonons within the silicon layer.

In region II there is one longitudinal phonon mode at 370 $cm^{-1}$. The relative atomic displacement pattern for this model is shown in Fig. 3(a). The bonds at the interface have displacements in opposite directions, making the mode sensitive to the interfacial force constants, though it is found that most of the frequency dependence of this mode comes from the thickness of the silicon layer. Because this frequency lies within the longitudinal-acoustic (LA) branch of bulk silicon, there is significant acousticlike excitation of the silicon atoms. In fact, this mode shows significant dispersion in the [ζ00] direction, as shown in Fig. 2. Because of this excitation of silicon atoms, this mode cannot be interpreted as being confined to the Si/Ge interface. This is consistent with the findings of Molinari *et al.*[25] Figure 3(b) shows the relative atomic displacements for the two transverse-interface (TI) modes. As shown in the figure, the atoms at the interface vibrate with opposite phase, with very little penetration into the surrounding layers, indicating strong confinement to the interface. Unlike the case depicted in Fig. 3(a), the displacements of the Si atoms away from the interface are quite small compared to the amplitude of vibration of the Si atoms at the interface. Because these modes are confined to the interface, their properties depend on the Si-Ge force constant. They do not show any dispersion in the growth direction and very little perpendicular to it. When the atomic-displacement patterns of these TI modes are examined closely, it is found that they exhibit "symmetric" and "antisymmetric" behavior,

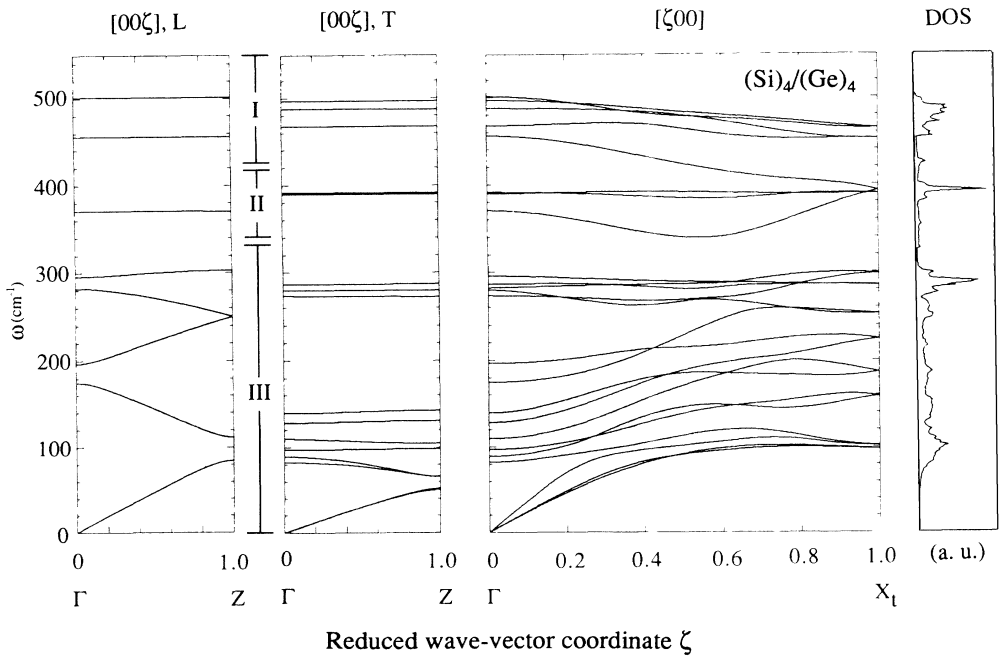


FIG. 2. Calculated phonon dispersions for a $(Si)_4/(Ge)_4$ superlattice grown on a [001] silicon substrate. The longitudinal (L) and transverse (T) dispersions in the growth direction are plotted separately. The dispersion perpendicular to the growth direction [ζ00] is plotted for all modes. The phonon DOS is shown on the far right. The different regions are discussed in the text.

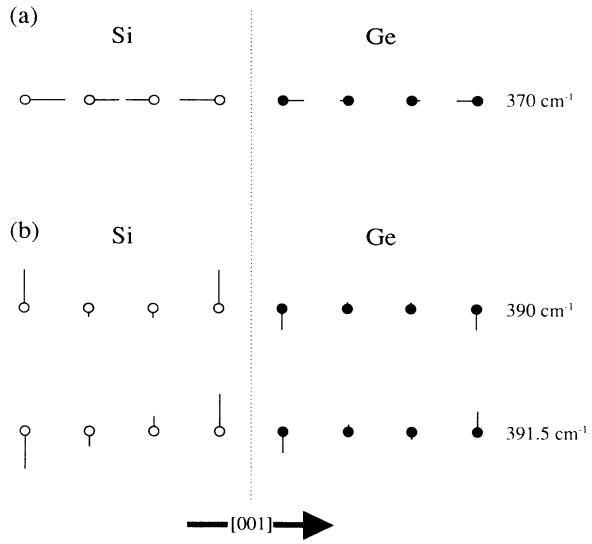


FIG. 3. Atomic-displacement patterns at the zone center for (a) the longitudinal mode and (b) the transverse-interface (TI) modes in region II in Fig. 2 for a $(Si)_4/(Ge)_4$ superlattice grown on a [001] silicon substrate. The "antisymmetric" TI mode is at 391.5 $cm^{-1}$ and the "symmetric" TI mode is at 390 $cm^{-1}$.

with the atoms of the same type at neighboring interfaces vibrating in phase or in antiphase to each other, respectively. For superlattices with $D_{2h}$ group symmetry, like $(Si)_4/(Ge)_4$ and $(Si)_8/(Ge)_4$, it has been shown[26,27] that the transverse-interface modes at the zone center vibrate with the same polarization vector. Because of this, these modes couple to form a symmetric-antisymmetric pair with an energy splitting that depends on the evanescent interfacial cross-coupling. This splitting is found to approach zero as the layer thicknesses are increased. We find that the coupling is more effective through the silicon layers than the germanium layers. The dispersionless behavior of these modes leads to a second large peak in the DOS at $\sim 390$ $cm^{-1}$.

In region III there are two longitudinal modes with zone-center energies around 290 $cm^{-1}$. At the zone center they appear as confined LO phonons in the germanium layer, similar to the confined LO phonons in the silicon layer. They show some finite dispersion away from the zone edge due to the overlap with the bulk LA-phonon branch in silicon. Below this are the well-known folded bulk LA modes of the superlattice. In the transverse polarization there are three TO modes confined to the Ge layer in the region of the bulk germanium optical phonon. Finally, there are the folded transverse-acoustic (TA) phonons. In the [$\zeta$00] direction the confined LO and TO germanium phonons and acoustic phonons all show some dispersion. At around 300 $cm^{-1}$ the DOS shows a peak due to the optical phonons confined to the germanium layer. Below it there are a series of broad peaks due to the folded acoustic phonons.

### C. Interface modes

In order to explore how the behavior of the interface mode varies with layer thicknesses, we modeled a $(Si)_8/(Ge)_4$ superlattice on a [001] silicon substrate. Figure 4 shows the dispersion relations and DOS for this configuration. We found that the longitudinal mode in region II now occurs at 390 $cm^{-1}$ and had similar character to the longitudinal mode at 370 $cm^{-1}$ in the $(Si)_4/(Ge)_4$ structure. When superlattices with thicker silicon layers were modeled, it is found that this mode continued to move up in frequency for silicon layers less than 12 monolayers thick, and remained fairly constant for thicker layers. Again, there was significant dispersion of

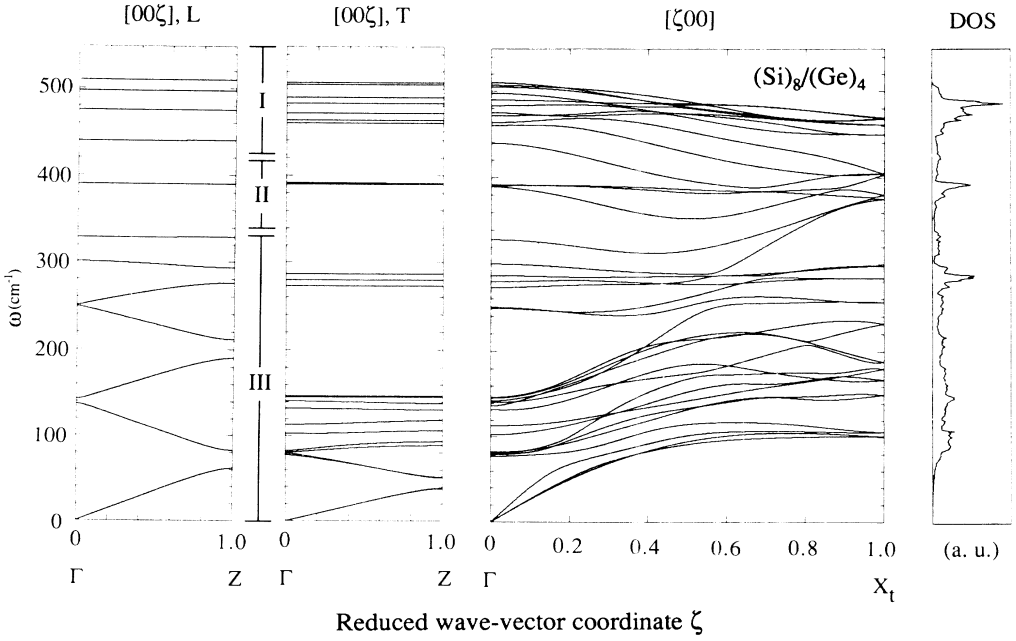


FIG. 4. Same as Fig. 2, except for a $(Si)_8/(Ge)_4$ superlattice grown on a [001] silicon substrate.

this mode in the [ζ00] direction, indicating a lack of confinement. The two TI modes occur at the same frequency as the TI modes in the $(Si)_4/(Ge)_4$ superlattice. The splitting between these two modes is the same, indicating that the majority of the interfacial coupling is through the germanium layer, whose thickness remained constant. This splitting was observed to disappear for germanium layers thicker than 4 monolayers. Along the in-plane direction, the TI phonons show small but finite dispersion. The DOS around 390 $cm^{-1}$ shows a peak which is due to the interface phonons and the longitudinal mode.

### D. Confined modes

In a Si/Ge superlattice the dominant mechanism for first-order Raman scattering is deformation-potential scattering. The $Z(XY)\bar{Z}$ scattering configuration is used to observe the longitudinal phonons polarized in the growth direction. Information on the bulk optical-phonon dispersions can be gained from plotting the experimental positions of the confined optical modes in a superlattice against an effective confined wave vector. The magnitude of this wave vector depends on the penetration depth of the confined optical phonon in the surrounding material.

To assess the degree to which LO phonons are confined in the silicon layer for a Si/Ge SLS grown in the [001] direction, the frequencies of the confined LO modes in a $(Si)_{20}/(Ge)_4$ superlattice grown on a silicon substrate in the [001] direction were calculated, and are plotted in Fig. 5 against their effective wave vector, given by the relation[16]

$$q = n\pi/d \ , \tag{9}$$

where $d$ is the nominal thickness of the layer the phonon is confined within, and $n$ is an integer greater than or equal to 1. Also shown is the calculated LO dispersion curve for pure, unstrained bulk silicon. It is readily apparent from the figure that the frequencies of the confined modes become progressively lower than expected for larger effective wave vectors. In effect, the effective layer thickness "seen" by the modes becomes larger than the actual thickness of the silicon layers for the higher-order modes. This seems to indicate that penetration into the adjacent germanium layers cannot be neglected for these modes. The increase in the penetration depth for modes with effective wave vectors near the zone edge can be explained qualitatively by noting that if there is any penetration at all, then waves with a larger effective wave vector will have a larger amplitude of vibration at the interface than waves with a lower effective wave vector. This larger vibrational amplitude at the interface would then need a longer distance to decay across the interface. Thus, the penetration depth for modes near the zone edge is greater than the penetration depth of modes near the zone center. An increased sensitivity of higher-order confined phonon modes to the interface properties has also been noted by Fasol *et al.*[28] This behavior is verified in Fig. 6, which shows the atomic-displacement patterns

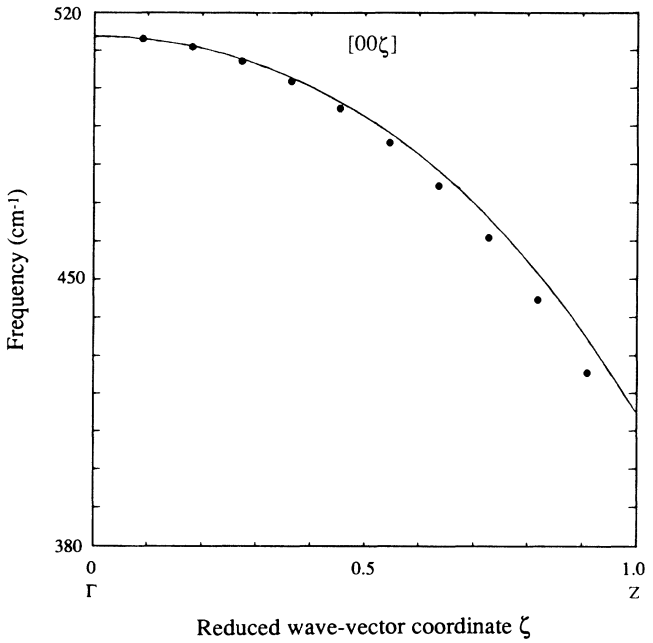


FIG. 5. Frequencies of confined silicon LO-phonon modes in a $(Si)_{20}/(Ge)_4$ SLS grown in the [001] direction on a silicon substrate plotted against the effective wave vector predicted by Eq. (9) (solid points). The calculated bulk LO dispersion curve for silicon is plotted as a solid line for comparison.

for the atoms in the immediate vicinity of the interface for the lowest-order confined LO mode at 513 $cm^{-1}$ and the highest-order confined LO mode at 425 $cm^{-1}$. Note that the magnitude of the displacements of the plane of silicon atoms at the interface is nearly negligible for the mode at 513 $cm^{-1}$, while it is quite significant for the mode at 425 $cm^{-1}$, which is consistent with our analysis.

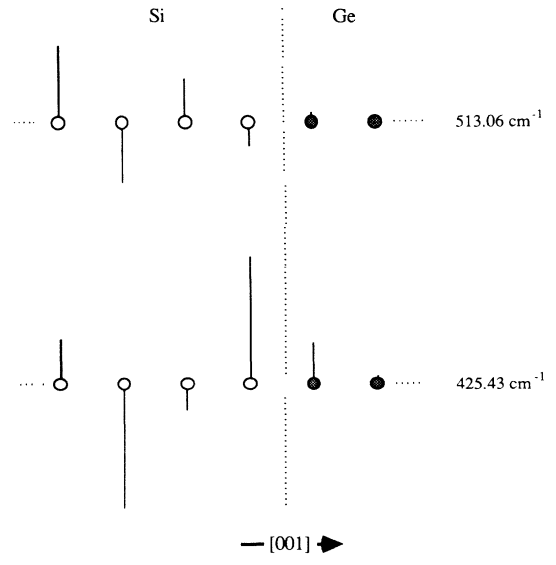


FIG. 6. Atomic displacements in the immediate area around the interface for the highest- and lowest-order silicon confined LO modes in Fig. 5.

To further support our conclusion that penetration into adjacent layers is responsible for the discrepancy in Fig. 6, the same calculation was performed with all the parameters the same, except that the mass of the germanium atoms was increased so as to be effectively infinite. As a result, the calculated frequencies of the confined modes mapped directly onto the bulk dispersion curve as per Eq. (9), and the atomic-displacement patterns showed that there was zero penetration into the fictitious "germanium" layer for any of the confined silicon LO modes.

When the frequencies of the confined silicon modes [$(\bar{1}10)$ polarization] in a $(Si)_{15}/(Ge)_3$ SLS grown in the [110] direction on a silicon substrate were calculated and plotted against the effective wave vector predicted by Eq. (9), it was found that, unlike the situation for [001] growth, the frequencies mapped exactly onto the calculated $\Sigma_2(O)$ dispersion curve for pure, unstrained silicon, as is shown in Fig. 7. The atomic-displacement patterns for these modes verified that the motion of germanium atoms in the plane directly adjacent to the interface is negligible, implying that confinement of phonons with $(\bar{1}10)$ polarization in the silicon layers is quite complete. The same type of behavior was noted for various silicon layer thicknesses. Similarly, we found that the confinement of phonons with $(\bar{1}10)$ polarization in germanium layers is also very nearly complete, and mapped directly onto the calculated $\Sigma_2(O)$ dispersion curve for pure, unstrained germanium. Experimentally, the mapping of observed phonon modes to bulk dispersion data has also shown excellent agreement for Si/Ge SLS's grown in the [110] direction.[19]

One possible qualitative explanation for the different degrees of confinement for the two different growth directions may arise from the different bonding geometries at the interface. For [110] growth, each atom at the interface has one nearest neighbor across the interface, two of which lie in the same plane, and one nearest neighbor in the adjoining layer away from the interface, providing only one direct bond coupling the motion of an atom at the interface with the motion of the atoms across the interface. For layers grown in the [001] direction, each atom at the interface has two nearest neighbors across the interface, increasing the number of direct paths to couple the vibrations of atoms across the interface.

### E. Comparison with experiment

The first-order Raman spectra of $(Si)_4/(Ge)_4$ and $(Si)_8(Ge)_4$ SLS's grown in the [001] direction on a silicon substrate are shown in Figs. 8(a) and 8(b), respectively, for the energy range between 480 and 550 $cm^{-1}$. The calculated positions of the $n=1$ confined modes are indicated in the figure, after correcting for temperature. The Raman spectra were taken using a $Kr^+$ laser, with the scattered light being detected by a DILOR triple-grating multichannel Raman spectrometer in the $Z(X,Y)\bar{Z}$

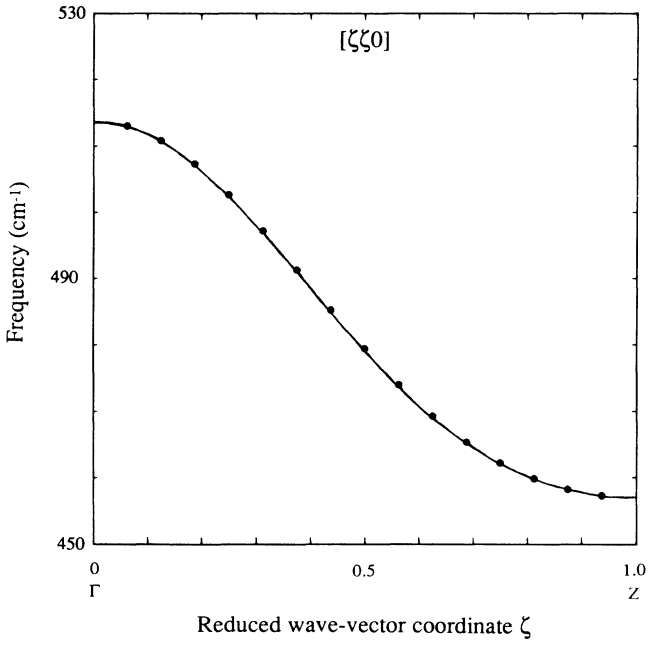


FIG. 7. Frequencies of confined silicon transverse phonon modes with $(\bar{1}10)$ polarization in a $(Si)_{15}/(Ge)_3$ SLS grown in the [110] direction on a silicon substrate, plotted against the effective wave vector predicted by Eq. (9) (solid points). The calculated bulk $\Sigma_2(O)$ dispersion curve for bulk silicon is plotted as a solid line for comparison.

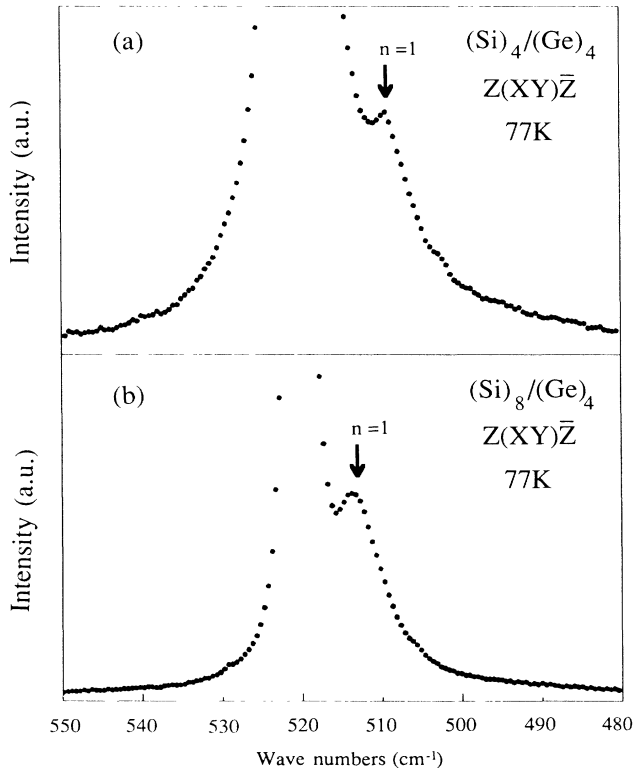


FIG. 8. Measured Raman spectra taken in the $Z(X,Y)\bar{Z}$ configuration for (a) a $(Si)_4/(Ge)_4$ SLS grown in the [001] direction on a silicon substrate, and (b) a $(Si)_8/(Ge)_4$ SLS grown in the [001] direction on a silicon substrate. The calculated position of the $n=1$ confined phonon in the silicon layers, adjusted for temperature, is indicted by the arrows in the figures.

configuration. The samples were held in a vacuum on the cold finger of a cryostat cooled to 77 K.

The large truncated peaks centered at 521 $cm^{-1}$ are the bulk-phonon peaks from the silicon substrate. For the $(Si)_4/(Ge)_4$ sample, there is a second peak at $\sim 509$ $cm^{-1}$ due to the $n=1$ confined mode of the superlattice. These spectra are equivalent to data published elsewhere[31,32] for $(Si)_4/(Ge)_4$. It is important to note that because the silicon layers are unstrained the secondary peak can be interpreted to arise solely because of confinement effects, and not some strain-induced shift of the bulk spectra. Similarly for the $(Si)_8/(Ge)_4$ sample there is a secondary peak at $\sim 514$ $cm^{-1}$ due to the $n=1$ mode. The computed positions for this mode in both structures is approximately 8 $cm^{-1}$ less than what was observed experimentally. This can be explained[33] by noting that the force constants used in our calculations were fitted to neutron-scattering data taken at room temperature, while the Raman spectra were taken at 77 K. After correcting for this temperature difference, the difference between the predicted and experimental positions is less than 1 $cm^{-1}$, indicating a strong quantitative agreement between our calculations and experiment. In the backscattering configuration, the $n=1$ mode is only confined optical-phonon mode that can be observed unambiguously for the short-period superlattices that we have investigated.

## V. SUMMARY

Raman scattering from phonons is currently an important technique for the characterization of Si/Ge superlattices. Si/Ge superlattices promise to expand the frontiers of silicon technology. Strain perturbs the properties of Si/Ge SLS's, adding a new and powerful degree of freedom which may potentially be used in the design of novel devices and structures. The present work has presented calculations made using a modified version of the valence-force-potential model (VFPM), predicting the nature of the vibrational spectra for SLS's grown in the [001] and [110] directions. Our model is fully three dimensional and incorporates strain effects for SLS's grown in the [001] directions. The VFPM has been used successfully to quantitatively model the phonon dispersion relations for bulk silicon and germanium. We presented analytical expressions for the expected frequency shifts due to strain in epitaxial layers. Our model precisely reproduces these frequency shifts. We have shown that the dispersion relations for [001] superlattices fall into bands which are closely related to the bulk vibrational spectra of the constituent materials. We found that the transverse-interface modes in [001] SLS's significantly couple between layers for silicon sheet thicknesses of less than 12 monolayers and for germanium layers less than 4 monolayers thick. Also, by comparing the calculated frequencies of confined phonons and their effective wave vector predicted by theory, we found that the penetration depth of confined phonons into adjacent layers was nearly zero for SLS's grown in the [110] direction, while it was significant for SLS's grown in the [001] direction. We postulate that this is due to the differing number of nearest-neighbor interactions across the interface for the two different growth directions. Our calculations thus indicate that penetration in adjacent layers may cause an appreciable deviation of the confined phonon energies versus effective confinement wave vector from the bulk-phonon dispersion curve. We presented measured Raman spectra for $(Si)_4/(Ge)_4$ and $(Si)_8/(Ge)_4$ samples that clearly showed the $n=1$ confined LO mode in the silicon layers. We showed that the predicted energy of these confined modes are within 1 $cm^{-1}$ of the measured experimental values after adjusting for temperature, confirming that our model, with its three-dimensional nature, can be used to quantitatively predict the nature of confined optical phonons in Si/Ge SLS's.

## ACKNOWLEDGMENTS

One of us (R.A.G.) gratefully acknowledges the financial support provided by the Winston Churchill Foundation of America and the Office of Naval Research. Another (J.D.W.) would like to acknowledge the support of the Science and Engineering Research Council and British Telecom. The authors express their thanks to H. Brugger for helpful discussions and the communication of results prior to publication, to M. Gell for useful discussions, and to the Rutherford Appleton Laboratories for the allocation of Cray computing time. We are grateful to the Director of Research and Technology of British Telecom for permission to publish this paper.

*Present address: Massachusetts Institute of Technology, Department of Electrical Engineering and Computer Science, Cambridge, MA 02139.

[1]For reviews, see B. Jusserand and M. Cardona, in *Light Scattering in Solids V,* edited by M. Cardona and G. Guntherödt (Springer-Verlag, Berlin, 1989), p. 49; R. People, IEEE J. Quantum Electron. **QE - 22**, 1696 (1986).

[2]K. Eberl, G. Krötz, R. Zachai, and G. Abstreiter, J. Phys. (Paris) Colloq. **48**, C5-329 (1987).

[3]H. Brugger, G. Abstreiter, H. Jorke, H. J. Herzog, and E. Kasper, Phys. Rev. B **33**, 5928 (1986).

[4]H. Brugger, H. Reiner, G. Abstreiter, H. Jorke, H. J. Herzog, and E. Kasper, Superlatt. Microstruct. **2**, 451 (1986).

[5]D. J. Lockwood, M. W. C. Dharma-Wardana, J. -M. Baribeau, and D. C. Houghton, Phys. Rev. B **35**, 2243 (1987).

[6]J. C. Tsang, S. S. Iyer, and S. L. Delage, Appl. Phys. Lett. **51**, 1732 (1987).

[7]S. S. Iyer, J. C. Tsang, M. W. Copel, P. R. Pukite, and R. M. Tromp, Appl Phys. Lett. **54**, 219 (1989).

[8]A. Fasolino and E. Molinari, J. Phys. (Paris) Colloq. **48**, C5-569 (1987).

[9]R. A. Ghanbari and G. Fasol, Solid State Commun. **70**, 1025 (1989).

[10]M. I. Alonso, M. Cardona, and G. Kanellis, Solid State Commun. **69**, 479 (1989).

[11]J. White, G. Fasol, R. A. Ghanbari, C. J. Gibbings, and C. G. Tuppen, Thin Solid Films **183**, 71 (1989).

[12]M. I. Alonso, F. Cerdeira, D. Niles, M. Cardona, E. Kasper,

and H. Kibbel, J. Appl. Phys. **66**, 5645 (1989).
[13]H. L. McMurry, A. W. Solbrig, Jr., J. K. Boyter, and C. Noble, J. Phys. Chem. Solids **28**, 2359 (1967).
[14]G. Fasol, M. Cardona, W. Hönle, and H. G. von Schnering, Solid State Commun. **52**, 307 (1984).
[15]R. Tubino, L. Piseri, and G. Zerbi, J. Chem. Phys. **56**, 1022 (1972).
[16]A. K. Sood, J. Menendez, M. Cardona, and K. Ploog, Phys. Rev. Lett. **54**, 2111 (1985).
[17]B. Jusserand and D. Paquet, Phys. Rev. Lett. **56**, 1752 (1986).
[18]A. K. Sood, J. Menendez, M. Cardona, and K. Ploog, Phys. Rev. Lett. **56**, 1753 (1986).
[19]E. Friess, H. Brugger, K. Eberl, G. Krotz, and G. Abstreiter, Solid State Commun. **69**, 899 (1989).
[20]F. Cerdeira, A. Pinczuk, J. C. Bean, B. Batlogg, and B. A. Wilson, Appl. Phys. Lett. **45**, 1138 (1984).
[21]E. Anastassakis, A. Pinczuk, E. Burstein, F. H. Pollak, and M. Cardona, Solid State Commun. **8**, 133 (1970).
[22]A. W. Solbrig, Jr., J. Phys. Chem. Solids **32**, 1761 (1971).
[23]F. Cerdeira, C. J. Buchenauer, F. H. Pollak, and M. Cardona, Phys. Rev. B **5**, 580 (1972).
[24]See also M. Cardona, in *Lectures on Surface Science,* edited by G. R. Castro and M. Cardona (Springer-Verlag, Berlin, 1987), p. 2.
[25]E. Molinari and A. Fasolino, Appl. Phys. Lett. **54**, 1220 (1989).
[26]M. Cardona, in *Proceedings of the NATO Advanced Research Workshop on Spectroscopy of the Semiconductor Microstructures, Venice, 1989,* Vol. 206 of *NATO Advanced Study Institute, Series B: Physics,* edited by G. Fasol, A. Fasolino, and P. Lugli (Plenum, New York, 1989).
[27]G. Kannelis, in Ref. 26.
[28]G. Fasol, M. Tanaka, H. Sakaki, and Y. Horikoshi, Phys. Rev. B **38**, 6056 (1988).
[29]A. A. Urusovskaya, in *Modern Crystallography IV — Physical Properties of Crystals,* Vol. 37 of *Springer Series in Solid-State Sciences,* edited by L. A. Shuvalov (Springer-Verlag, Berlin, 1987).
[30]M. Chandrasekhar, J. B. Renucci, and M. Cardona, Phys. Rev. B **17**, 1623 (1978).
[31]M. Ospelt, W. Basca, J. Hons, K. A. Mädor, and H. von Känel, Superlatt. Microstruct. **5**, 71 (1989).
[32]J. Menéndez, A. Pinczuk, J. Bevk, and J. P. Mannaerts, J. Vac. Sci. Technol. B **6**, 1306 (1988).
[33]T. R. Hart, R. L. Aggrawal, and B. Lax, Phys. Rev. B **1**, 638 (1970).

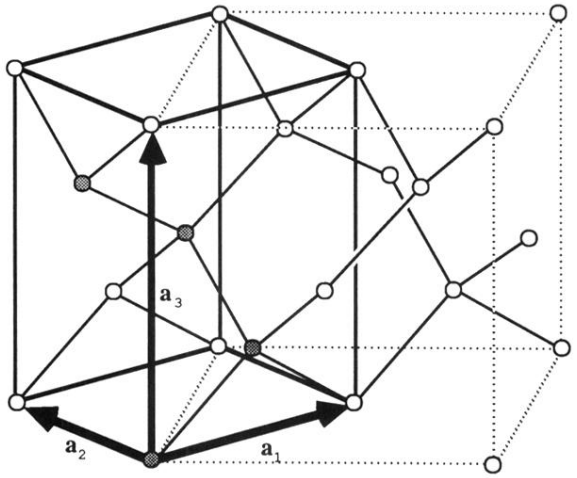


FIG. 1. Unit cell used to generate superlattices in the [001] ($\mathbf{a}_3$) and [110] directions ($\mathbf{a}_1$). The shaded atoms are the four atoms in the unit cell. Note that there are two atoms per plane in the [110] direction and only one atom per plane in the [001] direction.

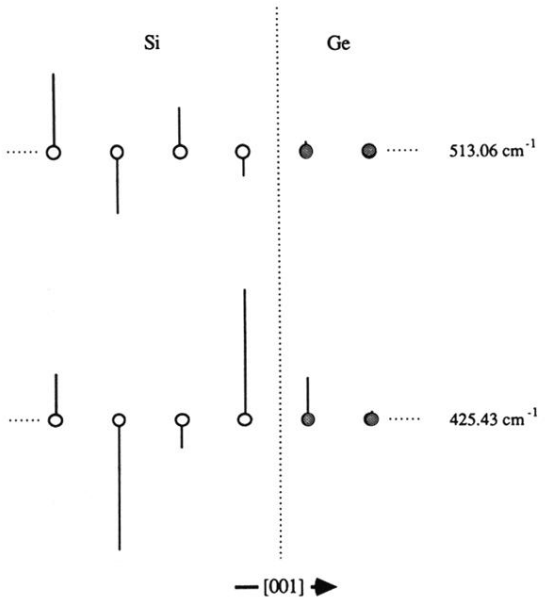


FIG. 6. Atomic displacements in the immediate area around the interface for the highest- and lowest-order silicon confined LO modes in Fig. 5.